文章编号：1001-9014(XXXX)XX-0001-09

DOI:10.11972/j.issn.1001-9014.XXXX.XX.001

A method for enhancing the performance of infrared filters based on rate-modulated deposition of germanium films

LIU Bao-Jian[1,2,4], LI Da-Qi[2], DUAN Wei-Bo[2,5*], YU De-Ming[2], CAI Qing-Yuan[2], YU Tian-Yan[2], JIANG Lin[2], YANG Yu-Ting[1,2], ZHUANG Qiu-Hui[4,5], ZHENG Yu-Xiang[1,3*]

(1. School of Information Science and Engineering, Fudan University, Shanghai 200433, China;
2. Shanghai Key Laboratory of Optical Coatings and Spectral Modulation, Shanghai Institute of Technical Physics, Chinese Academy of Sciences, Shanghai 200083, China;
3. Yiwu Research Institute of Fudan University, Fudan University, Zhejiang 322000, China;
4. State Key Laboratory of Extreme Photonics and Instrumentation, Zhejiang University, Zhejiang 310058, China;
5. College of Mechanical Engineering, Chongqing University of Technology, Chongqing 400054, China)

Abstract: This study systematically investigated the influence of deposition rate on the structure, broadband optical properties (1.0-13.0 μm), and stress characteristics of Germanium (Ge) films. Additionally, a method for enhancing the performance of infrared filters based on rate-modulated deposition of Ge films was proposed. The optical absorption of Ge films in the short-wave infrared (SWIR) and long-wave infrared (LWIR) bands can be effectively reduced by modulating the deposition rate. As the deposition rate increases, the Ge films maintain an amorphous structure. The optical constants of the films in the 1.0-2.5 μm and 2.5-13.0 μm bands were precisely determined using the Cody-Lorentz model and the classical Lorentz oscillator model, respectively. Notably, higher deposition rates result in a gradual increase in the refractive index. The extinction coefficient increases with the deposition rate in the SWIR region, attributed to the widening of the Urbach tail, while it decreases in the LWIR region due to the reduced absorption caused by the Ge-O stretching mode. Additionally, the films exhibit a tensile stress that decreases with increasing deposition rate. Finally, the effectiveness of the proposed fabrication method for an infrared filter with Ge films deposited at an optimized rate was demonstrated through practical examples. This work provides theoretical and technical support for the application of Ge films in high-performance infrared filters.

Key words: optical coatings, germanium film, optical absorption, infrared filter

基于锗薄膜速率调制沉积的红外滤光片性能提升方法

刘保剑[1,2,4], 李大琪[2], 段微波[2,5*], 余德明[2], 蔡清元[2], 于天燕[2], 蒋 林[2], 杨雨婷[1,2], 庄秋慧[4,5], 郑玉祥[1,3*]

(1. 复旦大学信息科学与工程学院,上海 200433;
2. 中国科学院上海技术物理研究所 上海市光学薄膜与光谱调控重点实验室,上海 200083;
3. 复旦大学义乌研究院,浙江 金华 322000;
4. 浙江大学极端光学技术与仪器全国重点实验室,浙江 杭州 310058;
5. 重庆理工大学机械工程学院,重庆 400054)

摘要:本文系统研究了沉积速率对锗(Ge)薄膜微观结构、宽波段光学特性(1.0~13.0 μm)及应力特性的影响,并提出了一种基于Ge薄膜速率调制沉积的红外滤光片性能提升方法。结果表明,通过调控沉积速率可有效

Received date: 2025-05-21, **revised date**: 2025-11-03 **收稿日期**:2025-05-21,**修回日期**:2025-11-03

Foundation items: Supported by the National Natural Science Foundation of China (62275053 , 62275256), National key Research and Development Program of China (. 2021YFB3701500), Youth Innovation Promotion Association of the Chinese Academy of Sciences (2023248), Eastern Talent Plan Youth Project 2022, and Shanghai Key Laboratory of Optical Coatings and Spectral Modulation (23dz2260500).

Biography: LIU Bao-Jian (1988-), male, Handan, master. Research area involves thin film optics and technology. E-mail: liubaojian@mail.sitp.ac.cn.

* **Corresponding author**: E-mail: ,duanweibo@mail.sitp.ac.cn; yxzheng@fudan.ac.cn

降低Ge薄膜在短波红外、长波红外波段的光学吸收。研究发现,随着沉积速率的提高,Ge薄膜保持非晶态结构。在光学常数表征方面,分别采用Cody-Lorentz模型和经典Lorentz振子模型精确计算了Ge薄膜在1.0~2.5 μm和2.5~13.0 μm波段的光学常数。随着沉积速率的提升,Ge薄膜折射率逐渐增大;在短波红外波段,Ge薄膜消光系数随沉积速率增加而上升,这是由于Urbach尾部展宽所致;而在长波红外波段,消光系数则随沉积速率增加而降低,主要归因于Ge-O键伸缩振动所导致的光学吸收强度在逐渐降低。此外,薄膜的拉伸应力随沉积速率升高而减小。最后,通过实例验证了所提出的基于Ge薄膜速率调制沉积提升红外滤光片性能方法的有效性。本文为Ge薄膜在高性能红外滤光片中的应用提供了理论依据和技术支撑。

关 键 词:光学薄膜;锗薄膜;光学吸收;红外滤光片

Introduction

Atmospheric transmission windows have significant applications in the field of space remote sensing, with the SWIR (1.0 – 3.0 μm) and LWIR (8.0 – 13.0 μm) bands serving as crucial operational wavelengths for remote sensing instruments[1-2]. As key optical components in space remote sensing systems, infrared filters are typically integrated with detector chips to enhance system signal-to-noise ratio and detection accuracy through selective transmission of specific infrared bands[3-4]. High transmittance and low optical absorption are essential performance indicators for infrared filters. Germanium is a crucial high-refractive-index film material for infrared applications, characterized by a broad infrared transparent region, high mechanical strength, and excellent chemical stability[5], making it widely used in infrared thin-film devices. Germanium is often combined with low-refractive-index materials, such as zinc selenide (ZnSe)[6-7], zinc sulfide (ZnS)[8-9], silicon monoxide (SiO)[10-11], and ytterbium fluoride (YbF_3)[12-13], to fabricate infrared filters, beam splitters, mirrors, and antireflection coatings. Although electron-beam evaporation has been widely adopted for Ge film deposition, significant optical absorption persists in the 1.8 – 2.5 μm and 10.5 – 12.5 μm bands, substantially limiting its applications in these bands. Therefore, developing an effective method to reduce optical absorption of Ge films in the SWIR and LWIR bands is crucial for enhancing the performance of infrared filters and expanding the engineering applications of Ge films in these spectral ranges.

Significant progress has been made in the study of the structure, optical and electrical properties of Ge films[14-18]. For instance, Liu *et al.* investigated the optical constants of Ge thin films from the visible region to the LWIR region using the Cody-Lorentz model and obtained bandgap and band-tail width of the films[19]. Similarly, Carney *et al.* measured the refractive indices of sputtered Ge films in the 2.5 – 13.0 μm band using Fabry-Perot transmission measurements[20]. Goh *et al.* employed spectroscopic ellipsometry and UV-Visible spectrophotometry to determine the bandgap and optical properties of Ge films with different thicknesses below 50 nm, which could be well described by the Forouhi-Bloomer model[21]. Notably, the optical and electrical properties of Ge films are significantly influenced by preparation processes, such as deposition temperature, ion beam assistance, and thermal annealing, which have been extensively investigated in previous studies[22-24]. However, limited research has explored how process conditions influence the broadband optical constants of Ge thin films and optical absorption in the SWIR and LWIR bands. Meanwhile, residual stress is a crucial mechanical property of optical thin films, as excessive residual stress can cause issues such as wrinkling, cracking, and delamination in thin-film devices[25]. Investigating the stress characteristics of Ge films is crucial for the design and preparation of infrared filters.

Deposition rate, as a critical process parameter in film fabrication, significantly influences the structure and optical properties of the films[26-28]. In this study, we systematically investigated the influence of deposition rate on the structure, broadband optical properties (1.0 – 13.0 μm), and stress characteristics of Ge films. The optical absorption of Ge films in the SWIR and LWIR bands can be effectively reduced by modulating the deposition rate. On this basis, we proposed a method for enhancing the performance of infrared filters based on rate-modulated deposition of Ge films. This work provides theoretical and technical support for the application of Ge films in high-performance infrared thin-film devices.

1 Methods

1.1 Physical dispersion models

Ferlauto *et al.* investigated band-tail absorption in amorphous semiconductor materials and incorporated it into a dispersion model[29]. They developed the Cody-Lorentz model and applied it to describe standard amorphous semiconductor materials. In this study, the Cody-Lorentz model was used to determine the optical constants of Ge films in the 1.0 – 2.5 μm band. The imaginary part (ε_i) of the dielectric function (ε) is expressed as follows[30, 31]:

$$\varepsilon_i(E)=\begin{cases}\dfrac{E_1}{E}\exp\left\{\dfrac{(E-E_t)}{E_u}\right\} & 0<E\leqslant E_t\\ G(E)L(E)=G(E)\dfrac{AE_0\Gamma E}{\left[\left(E^2-E_0^2\right)^2+\Gamma^2E^2\right]} & E>E_t\end{cases}, \tag{1}$$

$$G(E) = \frac{\left(E - E_g\right)^2}{\left(E - E_g\right)^2 + E_p^2}, \tag{2}$$

$$E_1 = E_t G\left(E_t\right) L\left(E_t\right), \tag{3}$$

where A, E_g, E_0, E, and Γ denote the Lorentz oscillator amplitude, bandgap energy, resonance energy, photon energy, and oscillator width, respectively. Here, E_t represents the boundary between the Urbach tail transitions and band-to-band transitions. The tail transition takes place when the photon energy is less than E_t, whereas the interband transition occurs when the energy exceeds E_t. E_p is the second transition energy (in addition to E_t). The absorption follows Lorentz linear absorption when the photon energy surpasses E_g+E_p. E_u, the Urbach tail width, is a key parameter for evaluating the disorder and defect density within the material structure. E_1 denotes the imaginary part of the dielectric constant, and ε_i remains continuous at $E = E_t$. $G(E)$ is a state density function, which is approximated as a constant dipole. The real part of the dielectric constant, ε_r, can be derived using the Kramers-Kronig transformation:

$$\varepsilon_r(E) = \varepsilon_\infty + \frac{2}{\pi} P \int_0^\infty \frac{E' \varepsilon_i(E')}{E'^2 - E^2} \mathrm{d}E'. \tag{4}$$

In this study, the optical constants of Ge films in the 2.5 – 13.0 μm band were determined using the classical Lorentz oscillator model. The real part (ε_r) and the imaginary part (ε_i) of the complex dielectric function (ε) are expressed as follows[32]:

$$\varepsilon = \varepsilon_r + \mathrm{i}\varepsilon_i = \varepsilon_\infty \left(1 + \sum_{j=1}^{m} \frac{A_j^2}{E_j^2 - E(E - \mathrm{i}\Gamma_j)}\right), \tag{5}$$

where ε_∞ represents the high-frequency dielectric constant, E_j is the central energy of the jth oscillator (in eV), A_j denotes the amplitude of the jth oscillator (in eV), Γ_j is the damping factor of the jth oscillator (in eV), and m represents the number of oscillators. The refractive index (n) and the extinction coefficient (k) can be determined using the following equations:

$$n = \sqrt{\frac{\sqrt{\varepsilon_r^2 + \varepsilon_i^2} + \varepsilon_r}{2}}, \tag{6}$$

$$k = \sqrt{\frac{\sqrt{\varepsilon_r^2 + \varepsilon_i^2} - \varepsilon_r}{2}}. \tag{7}$$

The measured transmittance (T) and reflectance (R) spectra were fitted by minimizing the mean squared error (MSE) value, and the MSE is defined as:

$$MSE = \sqrt{\frac{1}{2N - M} \sum_{j=1}^{N} \left[\left(T_j^{\exp} - T_j^{\mathrm{cal}}\right)^2 + \left(R_j^{\exp} - R_j^{\mathrm{cal}}\right)^2\right]}, \tag{8}$$

where N is the number of measured values, M denotes the number of fitting parameters, and "exp" and "cal" refer to the experimental and calculated data, respectively.

1.2 Sample preparation and characterization

The single-layer Ge film and infrared filter samples were prepared using a vacuum coater equipped with an optical monitoring system (LAB900, Leybold Optics, Germany). The samples were deposited by electron beam evaporation on ZnSe substrates with dimensions of Φ30 mm×3 mm. The substrates were polished, and the root-mean-square (RMS) surface roughness was less than λ/50 (λ=632.8 nm). Before deposition, vacuum chamber pressure was 2.0×10^{-3} Pa and the substrates were bombarded with ions for five minutes using a radio frequency (RF) ion source to enhance the film-substrate adhesion. The deposition rates for Ge films, controlled by a four-probe quartz crystal oscillator, were 0.3, 0.6, 1.0, 1.5, and 2.0 nm/s, respectively. The substrate temperature was maintained at 200°C during deposition.

The transmittance and reflectance spectra of the samples in the 1.0 – 2.5 μm band were measured using a UV-VIS-NIR spectrometer (Lambda 900, PerkinElmer, USA), and the measurement error was within 0.08%. The transmittance and reflectance spectra in the 2.5 – 13.0 μm band were measured using a Fourier transform infrared spectrometer (VERTEX 80, Bruker Co., Germany). The reflectance spectra of Ge films were measured using absolute reflectance measurements at 0° incidence for both the 1.0 – 2.5 μm and 2.5 – 13.0 μm bands. The optical constants and thicknesses of the Ge films were precisely determined by fitting the measured spectra of single-layer samples using physical dispersion models. The structure of the samples was analyzed by an X-ray diffractometer (XRD, Cu-Kα, Bruker, Germany). The measurement angle was 20° – 80°, and the step size (2θ) was 0.02°. A laser interferometer (VERIFIRE QPZ, Zygo Co., USA) was used to measure the curvature radii of ZnSe substrates before and after coating. The residual stress (σ) of Ge films was calculated using the Stoney equation[33-34]:

$$\sigma = \frac{E_s t_s^2}{6\left(1 - v_s\right) t_f} \left(\frac{1}{R_2} - \frac{1}{R_1}\right), \tag{9}$$

where E_s represents the Young's modulus of the substrate, v_s denotes the Poisson's ratio, t_f is the film thickness, t_s refers to the substrate thickness, and R_1 and R_2 are the curvature radii of the substrate before and after coating, respectively. The Young's modulus and Poisson's ratio of the ZnSe substrates are 67.2 GPa and 0.28, respectively.

2 Results and discussion

2.1 Film structure of Ge films

Figure 1 shows the grazing incidence X-ray diffraction (GIXRD) patterns of the Ge films deposited at different rates. No sharp diffraction peaks are observed, indicating that the films are non-crystalline and amorphous. A broad diffusion peak appears near 27° in the diffraction spectrum, suggesting the existence of short-range order in the film structure. Therefore, Eqs. (1 – 4) are applicable to the Ge thin films.

2.2 Optical properties of Ge films

Figures 2(a – d) illustrate the transmittance and reflectance spectra of Ge films deposited at different rates in the 1.0 – 2.5 μm and 2.5 – 13.0 μm bands. At wavelengths greater than 1.3 μm, the interference extre-

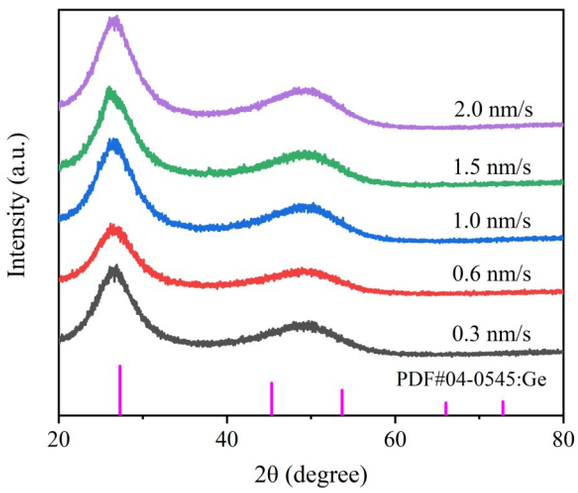

Fig. 1 GIXRD patterns of Ge films deposited at different rates.
图1 不同速率沉积的Ge薄膜掠入射X射线衍射图谱

ma are observed. Higher transmittance and reflectance at the same peak positions indicate lower optical absorption of the films. In the SWIR region, lower deposition rates result in higher transmittance and reflectance at the interference peaks. However, in the LWIR region (10.5 – 12.5 μm), higher deposition rates correspond to increased transmittance and reflectance. The short-wavelength absorption edge of Ge films exhibits a distinct redshift with increasing deposition rate, indicating changes in the optical bandgap. The transmittance and reflectance spectra were employed as targets for inverse calculations using the physical dispersion models described above to determine the optical constants of Ge films. Figures 3(a) and (b) present the experimental and fitted spectra of Ge film in the 1.0 – 2.5 μm and 2.5 – 13.0 μm bands, respectively. The fitted transmittance and reflectance spectra align well with experimental values, demonstrating that the models are sufficiently accurate for calculating the optical constants.

The optical bandgap and the Urbach tail width are two critical parameters for describing the energy band structure of thin films. The optical bandgap characterizes the short-wavelength absorption edge of the film and is a key parameter for assessing film absorption, while the Urbach tail width is essential for evaluating the structural disorder and defect density of the film. Parameters in the Cody-Lorentz model, including the optical bandgap E_g and the Urbach tail width E_u, can be obtained through inverse calculations of the transmittance and reflectance spectra. Table 1 summarizes the Cody-Lorentz model parameters of Ge films deposited at different rates in the 1.0 – 2.5 μm band. As the deposition rate increases, the bandgap E_g of Ge films decreases from 0.803 eV at 0.3 nm/s to 0.788 eV at 2.0 nm/s, consistent with the redshift of the short-wavelength absorption edge. Meanwhile, the Urbach tail width increases from 0.138 to 0.143 eV, reflecting a higher density of defect states in the film. A higher density of defect states corresponds to a wider band-tail width.

Figures 4(a) and (b) show the refractive indices and extinction coefficients of Ge films deposited at different rates in the 1.0 – 2.5 μm band, respectively. The

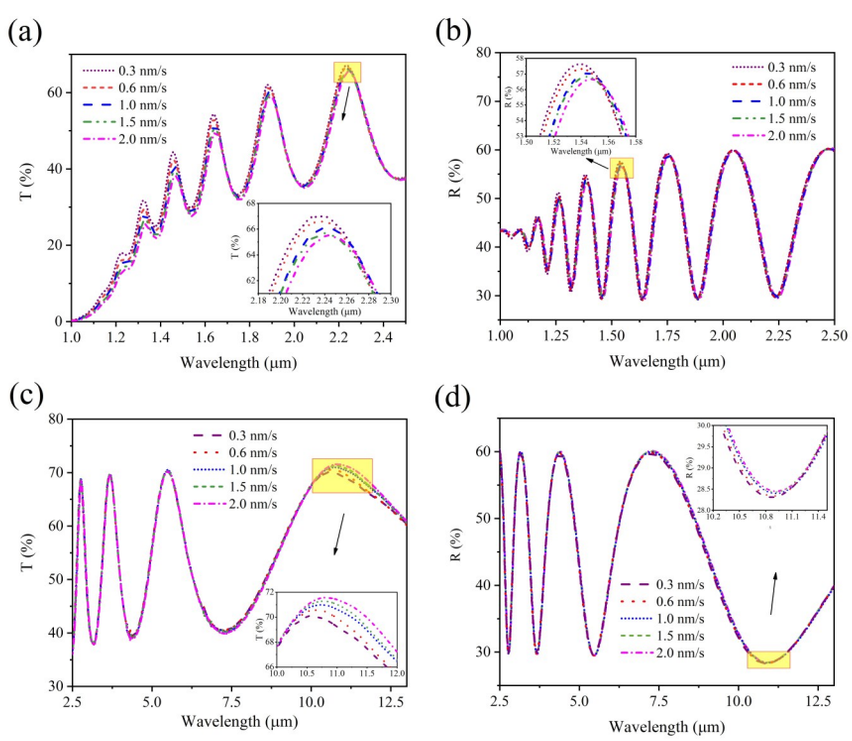

Fig. 2 (a) Transmittance and (b) reflectance spectra of Ge films deposited at different rates in the 1.0 – 2.5 μm band; (c) transmittance and (d) reflectance spectra of Ge films in the 2.5 – 13.0 μm band.
图2 不同速率沉积的Ge薄膜在1.0 ~2.5 μm波段的(a)透射谱和(b)反射谱;在2.5~13.0 μm波段的(c)透射谱和(d)反射谱

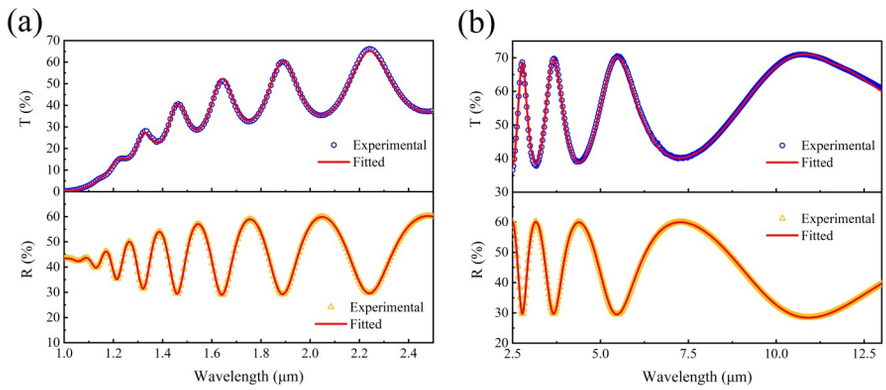

Fig. 3 Experimental (points) and fitted (lines) spectra of Ge film deposited at a rate of 1.0 nm/s in the (a) 1.0 – 2.5 μm and (b) 2.5 – 13.0 μm bands.
图3 沉积速率为1.0 nm/s的Ge薄膜在(a)1.0 – 2.5 μm和(b)2.5 – 13.0 μm波段的实验测量数据(点)与拟合曲线(线)

refractive indices decrease with increasing wavelength but gradually increase with deposition rate, likely due to the higher stacking density of the film. The extinction coefficients of Ge films also increase with deposition rate, which may result from the widening of the Urbach tail. Figures 4(c) and (d) illustrate the refractive indices and extinction coefficients of Ge films in the 2.5 – 13.0 μm band, respectively. Table 2 summarizes the classical Lorentz oscillator model parameters of Ge films. Notably, higher deposition rates result in higher refractive indices at the same wavelength. Additionally, a weak absorption peak appears near 11.6 μm, primarily due to the Ge – O stretching mode in Ge films[35-36]. The oxygen content in the film affects the infrared absorption, with higher oxygen concentrations leading to stronger absorption[37]. As the deposition rate increases, the intensity of the absorption peak gradually decreases. This trend may be attributed to the shorter contact time between Ge vapor molecules and residual oxygen in the vacuum chamber, leading to lower oxygen content in the film. The absorption peak disappears entirely when the deposition rate reaches 2.0 nm/s. Figure 5 shows the optical constants of Ge films deposited at 2.0 nm/s with reference data[14,38-40]. The optical constant dispersion properties of Ge films in this work exhibit consistency with published data, while the observed deviations in specific spectral regions are primarily attributed to the differences in thin-film deposition conditions and the distinct dispersion models employed for optical constants fitting.

2.3 Stress properties of Ge films

Residual stress is a crucial mechanical property of infrared optical coatings, significantly influencing their performance and environmental reliability. Thin films typically experience elastic mechanical stress both during and after deposition. Intrinsic stress, which is inherent to the deposition process, can be either tensile, where the film contracts parallel to its surface, or compressive, where the film expands parallel to its surface. The total residual stress, σ, is often analyzed in terms of three components[41-42], as follows:

$$\sigma = \sigma_{ext} + \sigma_{the} + \sigma_{int}, \tag{10}$$

where σ_{ext} represents the external stress caused by external forces, and σ_{the} and σ_{int} denote the thermal stress and

Table 1 Cody-Lorentz model parameters of Ge films deposited at different rates in the 1.0 – 2.5 μm band.
表1 不同速率沉积的Ge薄膜在1.0~2.5 μm波段的Cody-Lorentz模型参数

Sample	ε_∞	A (eV)	E_0 (eV)	Γ (eV)	E_g (eV)	E_p (eV)	E_t (eV)	E_u (eV)	Thickness(nm)
Ge-0.3nm/s	1.0	1137.7	1.679	3.5	0.803	6.033	0.224	0.138	1296.9
Ge-0.6nm/s	1.0	1082.2	1.657	3.5	0.802	5.767	0.240	0.139	1298.5
Ge-1.0nm/s	1.0	1060.9	1.637	3.5	0.801	5.622	0.244	0.142	1300.3
Ge-1.5nm/s	1.0	1087.0	1.620	3.5	0.797	5.663	0.251	0.142	1301.2
Ge-2.0nm/s	1.0	1121.1	1.611	3.5	0.788	5.761	0.261	0.143	1303.9

Table 2 Lorentz Oscillator model parameters of Ge films deposited at different rates in the 2.5 – 13.0 μm band.
表2 不同速率沉积的Ge薄膜在2.5~13.0 μm波段的Lorentz Oscillator模型参数

Sample	ε_∞	E_1 (eV)	A_1 (eV)	Γ_1 (eV)	E_2 (eV)	A_2 (10^{-3}eV)	Γ_2 (eV)	E_3 (eV)	A_3 (10^{-3}eV)	Γ_3 (eV)
Ge-0.3nm/s	12.0	1.214	0.764	0.0143	0.0654	9.440	0	0.107	4.058	0.018
Ge-0.6nm/s	12.0	1.214	0.768	0.0153	0.0654	0	0	0.107	3.615	0.019
Ge-1.0nm/s	12.0	1.214	0.773	0.0175	0.0654	0	0	0.107	2.268	0.014
Ge-1.5nm/s	12.0	1.214	0.778	0.0185	0.0654	0	0	0.107	1.652	0.015
Ge-2.0nm/s	12.0	1.214	0.782	0.0210	0.0654	0	0	0.107	0	0

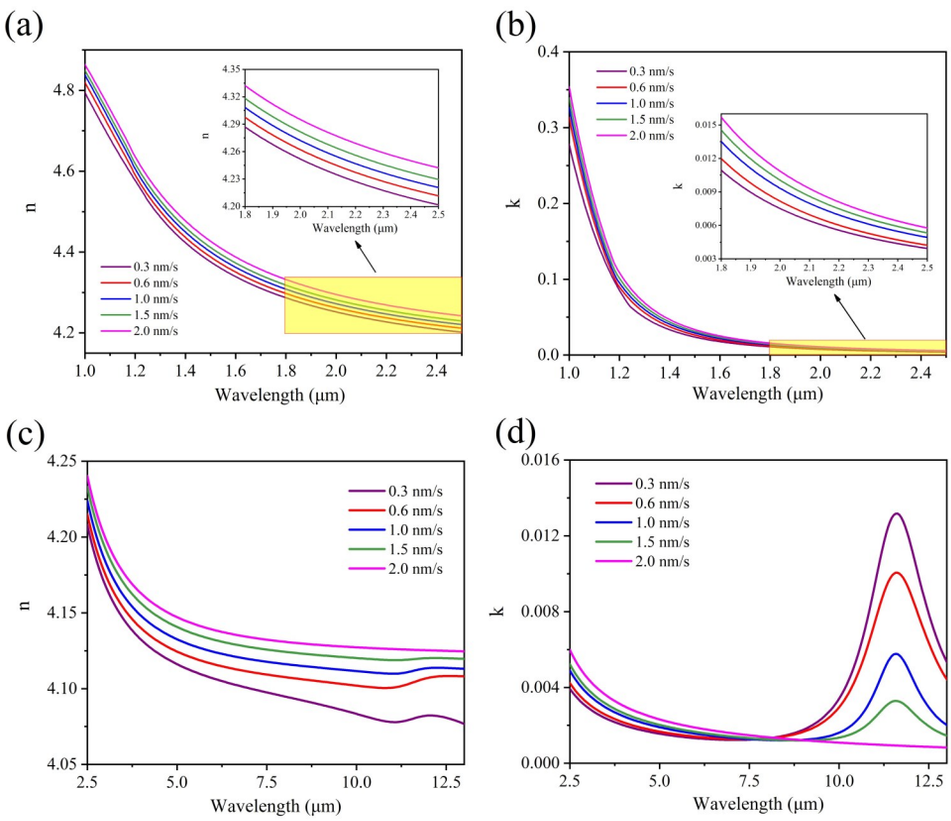

Fig. 4 (a) Refractive indices and (b) extinction coefficients of Ge films deposited at different rates in the 1.0 – 2.5 μm band; (c) refractive indices and (d) extinction coefficients of Ge films in the 2.5 – 13.0 μm band.
图4 不同速率沉积的Ge薄膜在1.0~2.5 μm波段的(a)折射率和(b)消光系数;在2.5~13.0 μm波段的(c)折射率和(d)消光系数

intrinsic stress, respectively. Thermal stress arises when significant differences exist in the thermal expansion coefficients between the film and substrate, which can be described as follows[43]:

$$\sigma_{\text{the}} = \left(\frac{E_{\text{f}}}{1 - v_{\text{f}}}\right)(\alpha_{\text{f}} - \alpha_{\text{s}})(T_1 - T_0), \tag{11}$$

where E_{f} and v_{f} denote the Young's modulus and Poisson's ratio of the film, while α_{f} and α_{s} represent the thermal expansion coefficients of the film and substrate, respectively; T_1 and T_0 refer to the temperatures during film deposition and measurement, respectively. For Ge material, the Young's modulus is 103.7 GPa, and the Poisson's ratio is 0.278. The thermal expansion coefficients of the Ge film and the ZnSe substrate are 5.8×10^{-6}/℃ and 7.6×10^{-6}/℃, respectively. The temperatures during film deposition and measurement are 200℃ and 25℃, respectively. All the Ge film samples in this study were deposited at the same temperature, so their thermal stresses can be approximated as equal. The thermal stress of Ge film on the ZnSe substrate is compressive and is calculated to be −45.2 MPa according to Eq. (11). Intrinsic stress is highly sensitive to the microstructure of the film, originating from the mode of film growth and the interactions within its microstructure, and can also be affected by contamination. Typically, intrinsic stress predominates in thin films and has been the focus of extensive research.

Figures 6(a – e) show the surface shapes of Ge film samples deposited at different rates and Fig. 6(f) presents the residual stresses of these samples. As shown in the figures, a positive stress value indicates tensile stress in the film, causing the coated surface to become concave. Conversely, a negative stress value represents compressive stress, resulting in a convex coated surface. Ge films deposited at different rates exhibit tensile stresses, indicating that the intrinsic stresses play a decisive role, while the residual stresses gradually decrease with increasing deposition rate. Generally, a higher refractive index for the same material corresponds to a higher packing density. Based on the fitting results of the refractive indices of Ge films, the stacking density of the films gradually increases with increasing deposition rate. For films deposited via evaporation, the kinetic energy of the deposited particles is closely related to the stacking density. Leplan and Pauleau *et al.* pointed out a direct correlation between the residual stress and packing density of the film[44]. At lower deposition rates, nucleation occurs slowly, and vapor molecules primarily condense on large aggregates, resulting in a looser film structure. In contrast, at higher deposition rates, the deposited particles reach the substrate with greater kinetic energy, facilitating the filling of voids and forming a denser film structure, i. e., a higher packing density. This structural transformation causes variations in the intrinsic stress within the film, shifting from tensile to compressive as

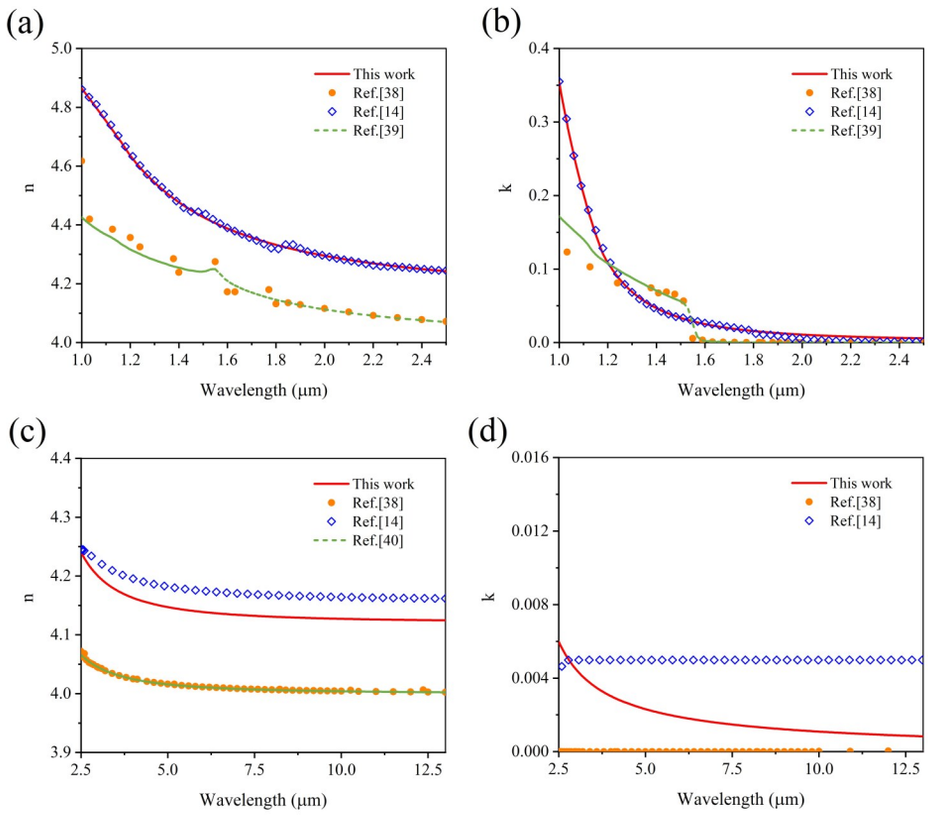

Fig. 5 Optical constants of Ge films deposited at 2. 0 nm/s with reference data: (a) refractive indices and (b) extinction coefficients in the 1. 0-2. 5 μm band; (c) refractive indices and (d) extinction coefficients in the 2. 5-13. 0 μm band.
图5 沉积速率为2. 0 nm/s的Ge薄膜光学常数与参考数据:在1. 0 ~2. 5μm波段的(a)折射率与(b)消光系数;在2. 5 ~13. 0μm波段的(c)折射率与(d)消光系数

the packing density increases[45]. Consequently, the residual stress macroscopically manifests as a decrease in tensile stress due to intrinsic stress effects with increasing deposition rate.

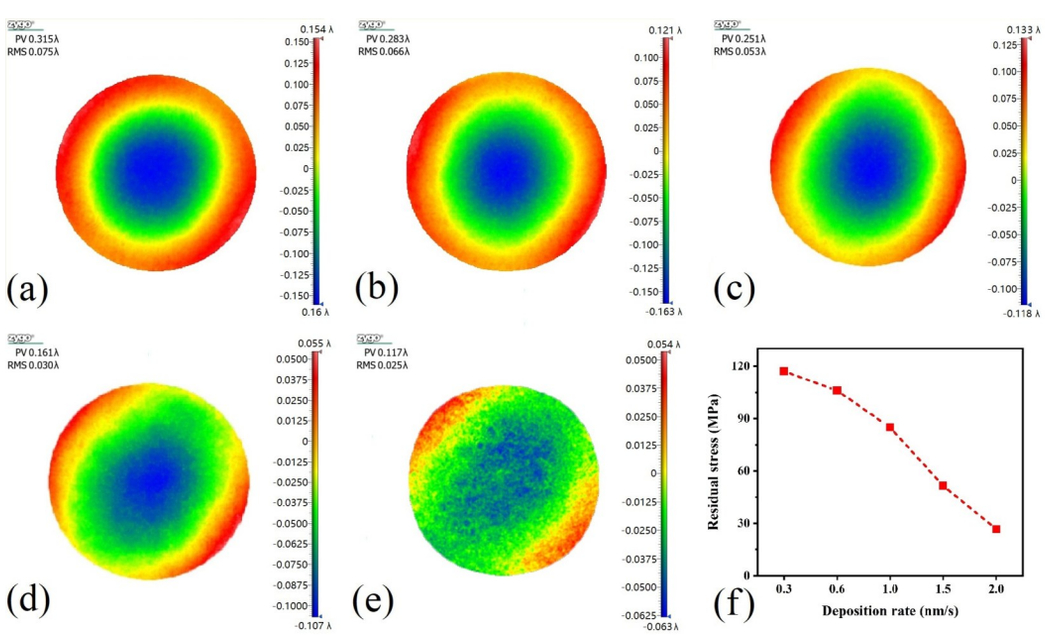

Fig. 6 Surface shapes of Ge film samples deposited at different rates: (a) 0. 3 nm/s, (b) 0. 6 nm/s, (c) 1. 0 nm/s, (d) 1. 5 nm/s, (e) 2. 0 nm/s; (f) residual stresses of Ge film samples.
图6 不同速率沉积的Ge薄膜样品面形图:(a)0. 3 nm/s,(b)0. 6 nm/s,(c)1. 0 nm/s,(d)1. 5 nm/s,(e)2. 0 nm/s;(f) Ge薄膜残余应力

2.4 Application of rate-modulated deposition of Ge films in infrared filters

The above research demonstrates that the optical absorption of Ge films in the SWIR and LWIR bands can be effectively reduced by modulating the deposition rate. Based on this finding, we proposed a rate-modulated method for fabricating infrared filters to enhance their performance in the SWIR and LWIR bands. In this study, the effectiveness of this method was verified through experimental demonstrations. Ge and ZnSe thin films were selected for the preparation of infrared filters in the SWIR and LWIR bands, respectively. The design structure of the infrared filters was Sub | 0.988H 2L 1H 1L 1H 1L 1H 2L 1H 1L 1H 1L 1H 1L 1H 2L 1H 1L 1H 1L 1H 2L 0.404H 0.861L | Air, where Sub refers to the ZnSe substrate; H and L denote the quarter-wave optical thicknesses of Ge and ZnSe layers, respectively; the values preceding H and L denote the optical thickness coefficients. The reference wavelengths were 2.13 μm and 10.8 μm, respectively. Additionally, an antireflection coating was applied to the backside of the substrate to eliminate the reflection effects. During the preparation of the infrared filters, Ge films were deposited at two rates: 0.3 and 2.0 nm/s, while other process conditions remained consistent. Figure 7(a) shows the transmittance spectra of the infrared filters prepared using Ge films deposited at two rates in the SWIR bands. At a deposition rate of 0.3 nm/s, the resulting infrared filter achieves a transmittance of 90.5%, which is 3% higher than that of the filter deposited at 2.0 nm/s. This improvement is due to the reduced optical absorption of the Ge films deposited at 0.3 nm/s in the SWIR band. Figure 7(b) presents the transmittance spectra of the infrared filters in the LWIR bands. The filter prepared with Ge films deposited at 2.0 nm/s exhibits a transmittance of 95.1%, which is 9% higher than that of the filter deposited at 0.3 nm/s. This enhancement is primarily attributed to the lower optical absorption of the Ge films deposited at 2.0 nm/s. Furthermore, the center wavelength of the infrared filter is 10.8 μm, and the increased thickness of the Ge film contributes to the higher optical absorption. These results suggest that low-rate deposition of Ge films is more suitable for SWIR filter fabrication, whereas high-rate deposition is preferable for LWIR filter fabrication.

3 Conclusion

To reduce the optical absorption of Ge films in the SWIR and LWIR bands and enhance the performance of infrared filters, we systematically investigated the influence of deposition rate on the structure, optical and stress properties of Ge films, and proposed a rate-modulated method to fabricate the filters. The results indicate that as the deposition rate increases, the Ge films maintain an amorphous structure. The optical constants of Ge films in the 1.0 – 2.5 μm and 2.5 – 13.0 μm bands were precisely determined using the Cody-Lorentz model and the classical Lorentz oscillator model, respectively. Higher deposition rates result in an increased refractive index. The extinction coefficient rises in the SWIR region with increasing deposition rate, attributed to the widening of the Urbach tail. Conversely, in the LWIR region (10.5 – 12.5 μm), the extinction coefficient decreases as higher deposition rates reduce the absorption caused by the Ge – O stretching mode. Additionally, the tensile stress in the films decreases with increasing deposition rate. Finally, the effectiveness of the proposed fabrication method for an infrared filter with Ge films deposited at an optimized rate was demonstrated through practical examples. This work is significant for advancing the application of Ge films in high-performance infrared thin-film devices.

Acknowledgment

This work was supported by the National Natural Science Foundation of China (Nos. 62275053 and 62275256), National key Research and Development Program of China (No. 2021YFB3701500), Youth Innovation Promotion Association of the Chinese Academy of Sciences (No. 2023248), Eastern Talent Plan Youth Project 2022, and Shanghai Key Laboratory of Optical

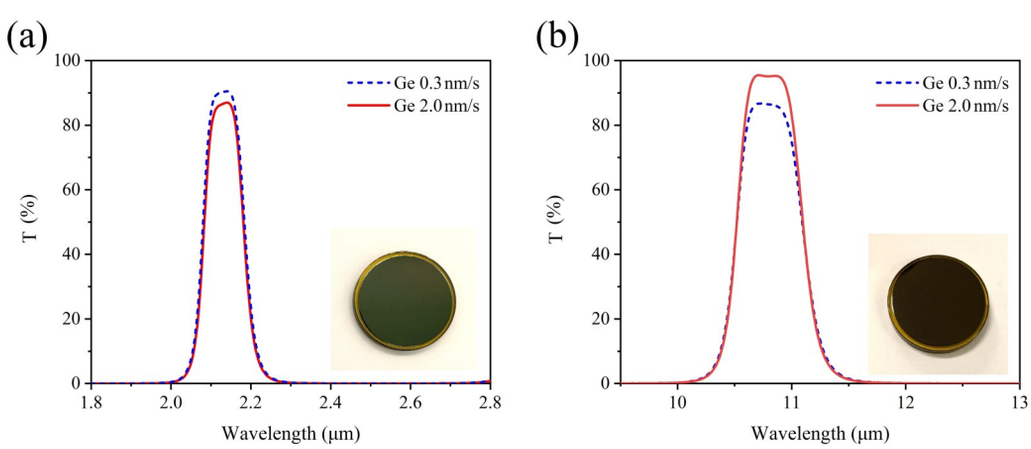

Fig. 7 Transmittance spectra of the infrared filters prepared using Ge films deposited at two rates in the (a) SWIR and (b) LWIR bands.

图7 采用两种沉积速率Ge薄膜制备的红外滤光片透射光谱:(a)短波红外波段;(b)长波红外波段

Coatings and Spectral Modulation (No. 23dz2260500).

References

[1] Schmit T J, Griffith P, Gunshor M M, et al. A closer look at the ABI on the GOES-R series[J]. Bulletin Of The American Meteorological Society, 2017, 98(4), 681 - 698.
[2] Zhang P, Zhu L, Tang S, et al. General comparison of FY-4A/AGRI with other GEO/LEO instruments and its potential and challenges in non-meteorological applications [J]. Frontiers of Earth Science, 2019, 6, 224.
[3] Hawkins G, Woods D, Sherwood R, et al. Infrared optical coatings for the EarthCARE Multispectral Imager[J]. Applied Optics, 2014, 53(30), 6983 - 6992.
[4] Wang K, Zhou S, Liu D, et al. Infrared linear variable optical filter with high dispersion coefficient and 2.65 to 4.65 μm band[J]. Optical Engineering, 2025, 64(4), 043103-043103.
[5] Rogalski A, Chrzanowski K. Infrared devices and techniques[J]. Opto-Electronics Review, 2002, 10(2), 111 - 136.
[6] Nazar A, Jasem N A, Abdalameer N K. Optimized design of optical filters for LWIR region[J]. Journal of Optics, 2024, 53(3), 1914-1917.
[7] Zhou S, Wang K, Liu D, et al. Research on infrared dual-color filters with 3.2 - 3.8 μm and 4.9 - 5.4 μm bands[J]. Chinese Optics, 2021, 14(3), 1 - 8.
[8] Hawkins G, Sherwood R, Djotni K, et al. Cooled infrared filters and dichroics for the Sea and Land Surface Temperature Radiometer[J]. Applied Optics, 2013, 52(10), 2125 - 2135.
[9] Zhou S, Zhang L, Guo F, et al. Design and fabrication of an integrated dual-channel thin-film filter for the mid-infrared[J]. Coatings, 2021, 11(7), 803.
[10] Gusev A G, Khasanov A M, Nurullin I Z, et al. Changes in optical thicknesses of Ge and SiO thin films and spectral characteristics of narrowband filters at cryogenic temperatures [J]. Journal of Optical Technology, 2022, 89(10), 595-599.
[11] Cai Y, Zhou S, Ma X, et al. Fabrication of short-wavelength infrared dual-band-pass filter based on combination of Fabry-Perot filters [J]. Applied Optics, 2016, 55(33), 9412 - 9416.
[12] Amochkina T, Trubetskov M. Designing broadband dispersive mirrors in the mid-infrared spectral range: a theoretical study [J]. Applied Optics, 2023, 62(7), B63-B72.
[13] Amotchkina T, Trubetskov M, Hussain S A, et al. Broadband dispersive Ge/YbF_3 mirrors for mid-infrared spectral range[J]. Optics Letters, 2019, 44(21), 5210 - 5213.
[14] Amotchkina T, Trubetskov M, Hahner D, et al. Characterization of e-beam evaporated Ge, YbF_3, ZnS, and LaF_3 thin films for laser-oriented coatings[J]. Applied Optics, 2020, 59(5), A40 - A47.
[15] Bundesmann C, Feder R, Wunderlich R, et al. Ion beam sputter deposition of Ge films: Influence of process parameters on film properties[J]. Thin Solid Films, 2015, 589, 487 - 492.
[16] Meng Z, Jin Z, Gururaj B A, et al. Germanium thin film formation by low-pressure chemical vapor deposition[J]. Journal of the Electrochemical Society, 1997, 144(4), 1423 - 1429.
[17] Wang X D, Wang H F, Chen B, et al. A model for thickness effect on the band gap of amorphous germanium film[J]. Applied Physics Letters, 2013, 102, 202102.
[18] Akl A A, Howari H. Nanocrystalline formation and optical properties of germanium thin films prepared by physical vapor deposition [J]. Journal of Physics and Chemistry of Solids, 2009, 70, 1337 - 1343.
[19] Liu H, Li S, Sun P, et al. Study on characterization method of optical constants of germanium thin films from absorption to transparent region [J]. Materials Science in Semiconductor Processing, 2018, 83, 58 - 62.
[20] Carney D J, Magnusson R. Refractive index of sputtered germanium films in the 2.5 - 13 μm infrared spectral region[J]. Optical Materials Express, 2019, 9(9), 3680 - 3690.
[21] Goh E S M, Chen T P, Sun C Q, et al. Thickness effect on the band gap and optical properties of germanium thin films[J]. Journal of Applied Physics, 2010, 107, 024305.
[22] Jiang L, Qin Y, Yu T, et al. NIR to LWIR dichroic beamsplitter designed and manufactured for space optical remote sensor[J]. Coatings, 2024, 14, 235.
[23] Ku S L, Lee C C, Tsai J S. Optical and structural properties of Ge films from ion-assisted deposition[J]. Thin solid films, 2008, 517, 704 - 708.
[24] Khan A F, Mehmood M, Rana A M, et al. Effect of annealing on structural, optical and electrical properties of nanostructured Ge thin films[J]. Applied Surface Science, 2010, 256, 2031 - 2037.
[25] Liu B, Li D, Duan W, et al. High-reliability infrared broadband thin-film polarizing beam splitter with ZnSe compensation layers[J]. Optics Express, 2024, 32(7), 10910 - 10924.
[26] Sun J, Li X, Zhang W, et al. Effects of substrate temperatures and deposition rates on properties of aluminum fluoride thin films in deep-ultraviolet region[J]. Applied Optics, 2012, 51(35), 8481 - 8489.
[27] Liebgott Q, Borroto A, Fernández-Gutiérrez Z, et al. Deposition rate controls nucleation and growth during amorphous/nanocrystalline competition in sputtered Zr-Cr thin films[J]. Journal of Alloys and Compounds, 2023, 936, 168258.
[28] Aoun Y, Benhaoua B, Benramache S, et al. Effect of deposition rate on the structural, optical and electrical properties of Zinc oxide (ZnO) thin films prepared by spray pyrolysis technique[J]. Optik, 2015, 126(20), 2481 - 2484.
[29] Ferlauto A S, Ferreira G M, Pearce J M, et al. Analytical model for the optical functions of amorphous semiconductors from the near-infrared to ultraviolet: applications in thin film photovoltaics[J]. Journal of Applied Physics, 2002, 92(5), 2424 - 2436.
[30] Price J, Hung P Y, Rhoad T, et al. Spectroscopic ellipsometry characterization of $Hf_xSi_yO_z$ films using the Cody - Lorentz parameterized model[J]. Applied Physics Letters, 2004, 85(10), 1701 - 1703.
[31] Němec P, Přikryl J, Nazabal V, et al. Optical characteristics of pulsed laser deposited Ge - Sb - Te thin films studied by spectroscopic ellipsometry[J]. Journal of Applied Physics, 2011, 109(7), 073520.
[32] Su W, Li B, Liu D, et al. The determination of infrared optical constants of rare earth fluorides by classical Lorentz oscillator model[J]. Journal of Physics D-Applied Physics, 2007, 40(11), 3343 - 3347.
[33] Stoney G G. The tension of metallic films deposited by electrolysis [J]. Proceedings of the Royal Society A, 1909, 82(553), 172 - 175.
[34] Tien C L, Zeng H D. Measuring residual stress of anisotropic thin film by fast Fourier transform[J]. Optics Express, 2010, 18(16), 16594 - 16600.
[35] Kaiser W, Keck P H, Lange C F. Infrared absorption and oxygen content in silicon and germanium[J]. Physical Review, 1956, 101(4), 1264.
[36] Davies G, Kohli K K, Clauws P, et al. Decay mechanism of the ν_3 865 cm^{-1} vibration of oxygen in crystalline germanium[J]. Physical Review B, 2009, 80(11), 113202.
[37] Litvinov V V, Svensson B G, Murin L I, et al. Determination of interstitial oxygen concentration in germanium by infrared absorption [J]. Journal of Applied Physics, 2006, 100, 033525.
[38] Palik E D. Handbook of optical constants of solids [M]. Academic press, 1998.
[39] Nunley T N, Fernando N S, Samarasingha N. Optical constants of germanium and thermally grown germanium dioxide from 0.5 to 6.6 eV via a multisample ellipsometry investigation[J]. Journal of Vacuum Science & Technology B, 2016, 34(6), 061205.
[40] Burnett J H, Kaplan S G, Stover E. Refractive index measurements of Ge [C]. Proc. SPIE, 2016, 9974, 222-232.
[41] Stolz C J, J. Taylor R, Eickelberg W K, et al. Effects of vacuum exposure on stress and spectral shift of high reflective coatings[J]. Applied Optics, 1993, 32(28), 5666 - 5672.
[42] Wang Y, Zhang Y G, Chen W L, et al. Optical properties and residual stress of YbF_3 thin films deposited at different temperatures[J]. Applied Optics, 2008, 47(13), C319 - C323.
[43] Marques F C, Wickboldt P, Pang D, et al. Stress and thermomechanical properties of amorphous hydrogenated germanium thin films deposited by glow discharge[J]. Journal of Applied Physics, 1998, 84(6), 3118 - 3124.
[44] Leplan H, Geenen B, Robic J Y, et al. Residual stresses in evaporated silicon dioxide thin films: Correlation with deposition parameters and aging behavior[J]. Journal of Applied Physics, 1995, 78(2), 962 - 968.
[45] Cen M, Zhang Y, Chen W, et al. Influences of deposition rate and oxygen partial pressure on residual stress of HfO_2 films [J]. Acta Physica Sinica, 2009, 58(10), 7025 - 7029.